Material Decomposition in Photon-Counting CT: A Deep Learning Approach Driven by Detector Physics and ASIC Modeling

Xiaopeng Yu[1], Qianyu Wu[3,1], Wenhui Qin[1], Tao Zhong[1], Mengqing Su[3,1], Jinglu Ma[2], Yikun Zhang[3], Xu Ji[3], Guotao Quan[2], Yang Chen[3], Yanfeng Du[2], Xiaochun Lai[1]

[1] School of Biomedical Engineering, ShanghaiTech University, Shanghai, China
laixch@shanghaitech.edu.cn
[2] Shanghai United Imaging Healthcare Co., Ltd, Shanghai, China
[3] School of Computer Science and Engineering, Southeast University, Jiangsu, China

Abstract. Photon-counting computed tomography (PCCT) based on photon-counting detectors (PCDs) stands out as a cutting-edge CT technology, offering enhanced spatial resolution, reduced radiation dose, and advanced material decomposition capabilities. Despite its recognized advantages, challenges arise from real-world phenomena such as PCD charge-sharing effects, application-specific integrated circuit (ASIC) pile-up, and spectrum shift, introducing a disparity between actual physical effects and the assumptions made in ideal physics models. This misalignment can lead to substantial errors during image reconstruction processes, particularly in material decomposition. In this paper, we introduce a novel detector physics and ASIC model-guided deep learning system model tailored for PCCT. This model adeptly captures the comprehensive response of the PCCT system, encompassing both detector and ASIC responses. We present experimental results demonstrating the model's exceptional accuracy and robustness. Key advancements include reduced calibration errors, enhanced quality in material decomposition imaging, and improved quantitative consistency. This model represents a significant stride in bridging the gap between theoretical assumptions and practical complexities of PCCT, paving the way for more precise and reliable medical imaging.

Keywords: Photon-counting CT · Image reconstruction · Deep learning · Material decomposition.

1 Introduction

Photon counting CT (PCCT) has been considered a revolutionary advancement in clinical CT technology in the recent decade [18]. Unlike traditional CT's energy-integrating ones, photon-counting detectors (PCDs) directly convert individual incident photons to charges and record counts according to their energies, which eliminates electronic noise. PCDs have multiple energy bins to

realize novel spectral CT imaging applications such as material decomposition, virtual monochromatic imaging, and K-edge contrast imaging [14,15]. Advantages of PCCTs include higher spatial resolution, better CNR, and a decrease in iodine contrast amount and radiation dose [7].

PCCT stands out by its ability to generate 'colorful' images [17]. It measures the interaction of different energy X-ray photons with tissues, akin to decomposing an optical image into RGB components in computer vision. PCCT can decompose human tissue images into several bases, such as water and bone, in a process known as material decomposition [5]. This technique has diverse clinical applications, including in CT angiography, blood pool imaging, urinary stone characterization, and more, thereby significantly enhancing diagnostic capabilities [1,10,11,12].

However, the intricacies of PCCT present significant challenges in accurately modeling system responses. Complexities arise from physics and signal processes, such as detector charge-sharing effects, ASIC (Application-Specific Integrated Circuit) pile-up effects, and Compton scattering [18]. These factors make it difficult to precisely model PCCT's response, leading to potential biases in material decomposition and a consequent degradation in image quality. Adding to these challenges is the variability in the behavior of individual detector pixels within the PCCT system. Even minor differences in reality, such as variations in ASIC dead time, play a significant role. Notably, these discrepancies are the primary causes of ring artifacts in material decomposition images.

In addressing the challenges inherent in PCCT material decomposition, two primary strategies are commonly adopted: image-domain and detector-domain methods [6]. Image domain methods can be summarized as two steps: 1) image reconstruction and 2) material decomposition [9,20]. However, image domain methods may amplify noise and a beam-hardening effect exists [8]. On the other hand, detector domain methods directly conduct material decomposition. However, it is challenging to accurately model those complex physics phenomena and build the correct relationship between material depths and system counts [13,19]. Recently, deep learning has emerged as a potential game-changer for PCCT. Yet, significant optimization is still required, notably in two key areas: first, the integration of domain knowledge. Many deep learning models are trained without incorporating critical physics and signal processing insights, leading to potential inaccuracies and an incomplete understanding of PCCT systems [2]. Second, the requirement for extensive training datasets. The need for large, comprehensive datasets that accurately represent clinical scenarios presents a substantial challenge [2], often unfeasible in real-world clinical settings.

In this paper, we propose a novel physics-guided material decomposition model for PCCT. The special features of our method can be summarized as follows: 1) Integration of extensive physics knowledge; 2) Leveraging deep learning for complex processes, such as detector/ASIC response; 3) Incorporating critical physics parameters, such as charge sharing effects and ASIC dead time, as inputs to our network. This novel approach allows for a two-phased training strategy, where the model is initially shaped by simulated data to capture the theoreti-

cal impacts of these parameters, followed by fine-tuning through experimental calibration to adjust for real-world deviations.

2 Method

The framework of our proposed method is illustrated in Fig. 1. Our methodology unfolds in four steps: 1) Dataset construction, where we compile and organize the necessary data; 2) Training of the Detector Net and ASIC Net, aimed at learning the nuances of photon counting detector and ASIC responses under various physics parameters; 3) Calibration to determine the optimal critical detector and ASIC physics parameters through experimental means; 4) estimating basis material depths.

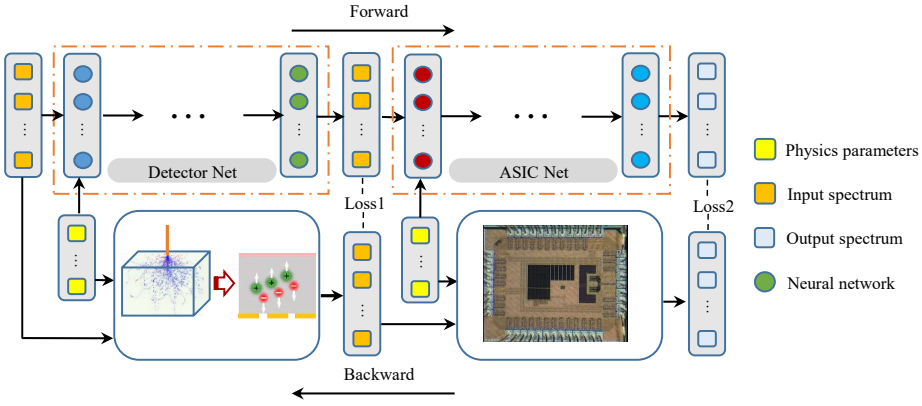

Fig. 1. Framework of our proposed method. Based on our PCCT full-chain model, we build a large dataset to simulate the system response under different physics parameters. We develop two neural networks, Detector Net and ASIC Net, designed to reflect the underlying physical processes of the PCCT system. These networks incorporate key physics parameters to simulate complex interactions within the system. When the network is trained, in the 'forward' process, given physics parameters, the network is expected to predict the bin counts of PCCT. In the 'backward' phase, given bin counts, material depth is back-traced.

2.1 Physics Simulation Model and Dataset Construction

We have developed a comprehensive PCCT Monte Carlo model. This model is specifically designed to simulate both the detector response and the ASIC response of the PCCT system. In our simulation, we meticulously incorporate the full signal processing chain. It includes X-ray energy deposition [4], charge transportation, and the charge-sharing effect, which are crucial for accurately

modeling the detector's behavior. Additionally, we account for signal generation, as well as various factors related to the ASIC, such as dead time and signal pile-up. Furthermore, the model integrates the intricacies of count trigger level, among other relevant parameters. By including these diverse elements, our Monte Carlo model aims to provide a robust and realistic representation of the PCCT system's operational dynamics.

The system response can be represented abstractly as follows:

$$S(E, \beta, l_f, L) = \beta N S_0(E) e^{-\mu_f(E) l_f} e^{-\mu L}, \tag{1}$$

$$\Lambda(L, P) = S(E, \beta, l_f, L) \circ D(E, P_1) \circ A(E, P_2), \tag{2}$$

where $S(E, \beta, l_f, L)$ is PCCT's tube initial spectrum $S_0(E)$ after (bowtie) filter attenuation l_f and tissue attenuation L, β is X-ray tube coefficient, N is the total number of photons, $A(E, P_2)$ is PCCT's ASIC response, $D(E, P_1)$ is PCCT's photon counting detector response, $\Lambda(L, P)$ is PCCT system counts of a single detector, which is the composite of spectrum, detector and ASIC response. L is tissue depths, P is related physics parameters.

In photon counting detector response $D(E, P_1)$. When X-ray photons arrive at the detector, the detector's semiconductor material (like CZT) will convert photons into free electrons and holes. Due to the strong electric field on both sides of the detector, electrons, and holes will move towards the positive and the negative side, and this procedure follows the electron transportation partial differential equations and hole transportation equations are similar:

$$\frac{\partial n_f}{\partial t} = \nabla \cdot J_n - \frac{n_f}{\tau_n}, \tag{3}$$

$$J_n = D_n \nabla n_f - n_f \mu_n \nabla \phi, \tag{4}$$

$$\frac{\partial n_t}{\partial t} = \frac{n_f}{\tau_n}, \tag{5}$$

where n_f is free electron distribution, n_t is trapped electron distribution, t is time, J_n is electron flux, τ_n is electron lifetime, D_n is electron diffusion coefficient, μ_n is electron mobility, and ϕ is electric potential.

In ASIC response $A(E, P_2)$, we detail the ASIC's operational workflow. The process begins as electrical currents from detector pixels are captured by a preamplifier, which then amplifies these signals into voltage readings. The energy of X-ray photons is deduced by analyzing these voltage signals. Throughout this modeling, factors such as dead time, signal pile-up, and shifts in count trigger levels are meticulously accounted for, ensuring a comprehensive representation of the ASIC's functionality.

2.2 Detector Net and ASIC Net

Employing the dataset we have meticulously compiled, our next step involves the development of both the Detector Net and ASIC Net. These networks are specially engineered to mirror the complex physics processes that are fundamental

to the operation of the PCCT system. The design of the inputs for these networks is a critical aspect, ensuring they accurately capture the essential elements of the system.

For the Detector Net, the principal input is the X-ray spectrum distributions, which are a result of attenuation by the bowtie filter and tissue materials. This input realistically reflects the scenarios encountered in PCCT scans, thus providing an authentic basis for simulation. Additionally, we integrate vital physics parameters, such as the charge-sharing coefficient, into the input. This coefficient is instrumental in determining the detector system's behavior. Consequently, the output of the Detector Net is a spectrum that has been altered according to the detector's response mechanisms, offering a representation of how the spectrum would appear to the PCCT system after interacting with the detector.

Similarly, the ASIC Net is structured around inputs that include the X-ray spectrum output from the Detector Net, along with critical physics parameters such as ASIC dead time, count trigger level, and pile-up coefficient. These parameters are pivotal in dictating the ASIC's response to the detected signals. The output of the ASIC Net, therefore, is the bin counts that have been processed through the ASIC response. This output encapsulates the final stage of the signal processing within the PCCT system, translating the physical interactions into quantifiable data suitable for image reconstruction and analysis.

In our experiment, our network consists of five convolutional layers with a kernel size of 3 and five fully-connected networks, each layer is followed by an activated function RELU. We choose the maximum log-Poisson as the loss function.

In summary, our objective for these networks is to yield accurate responses under varying physics parameters, effectively modeling the complex, non-linear dynamics of the PCCT system. This concept can be encapsulated in the equation:

$$\tilde{A}(L, P) = \tilde{S}(E, \beta, l_f, L) \circ D_\theta(E, P_1) \circ A_\theta(E, P_2), \tag{6}$$

where $\tilde{S}(E, \beta, l_f, L)$ is the empirical spectrum, D_θ and A_θ are Detector Net and ASIC Net. This formula demonstrates our networks' role in simulating the highly non-linear responses characteristic of the PCCT system.

2.3 Calibration

However, in experimental scenarios, the specific parameters of the PCCT system are not initially known. Therefore, calibration becomes essential to determine the optimal set of physics parameters. Once the Detector Net and ASIC Net are fixed, our task is to align the known system counts and the system's functional model with the real-world scenario. Essentially, given the system counts and the functional model of the system, we aim to ascertain the most accurate physics parameters that best fit the actual behavior of the PCCT system.

This calibration process is critical for ensuring that the deep learning model, which has been trained on simulated data, can effectively adapt and respond accurately in practical, experimental settings. By fine-tuning these parameters,

we enhance the model's capacity to replicate the complex dynamics of the PCCT system under various real-world conditions.

To express the calibration procedure mathematically, we can say

$$\tilde{P} = \arg\min_{P} Loss(\Lambda, \tilde{\Lambda}(L, P)), \tag{7}$$

and we can use the optimization method to find the optimal physics parameters $\tilde{P}$. In our paper, we use gradient descent to simplify the procedure.

2.4 Material Decomposition

Once the non-linear function $\tilde{\Lambda}(L, P)$ and its associated parameters, including material depths and other physics parameters, are established, we are equipped to predict the ideal counts of the PCCT system. This predictive capability is central to understanding and accurately modeling the system's behavior under various conditions.

Conversely, when we have the estimated nonlinear function $\tilde{\Lambda}$, along with the approximated physics parameters $\tilde{P}$, and the observed system counts, we can effectively reverse-engineer the process to determine the material depths $L = [l_1, \cdots, l_k]$, and $k = 2$ in this paper. This is achieved by solving the optimization problem:

$$\tilde{L} = \arg\min_{L} Loss(\Lambda, \tilde{\Lambda}(L, \tilde{P})). \tag{8}$$

In this optimization framework, our goal is to minimize the loss function, which measures the discrepancy between the actual system counts (Λ) and the counts predicted by our model ($\tilde{\Lambda}(L, P)$). By solving this problem, we can accurately trace back and determine the material depths.

By solving the optimization problem and finding the basis material depths, we can use traditional image reconstruction methods like filtered back projection (FBP) or iterative methods. In this paper, we use FBP as our image reconstruction algorithm.

3 Experiment

Utilizing a PCCT prototype system based on United Imaging's u960+, which has a large field of view and energy-sensitive photon-counting detectors of 2-mm-thick cadmium zinc telluride (CZT) with two energy bins ([30, 60] and 60 keV above), we conducted a series of calibration and material decomposition experiments. The tube current is 200 mA, and the tube voltage is 140 kVp. Compared with the typical methods, our method demonstrates reduced calibration errors, enhanced quality in material decomposition imaging, and improved quantitative accuracy.

3.1 Compared Methods

Our method is evaluated against several established approaches:
Filtered back-projection (FBP): This involves applying FBP directly to raw PCCT counts. For comparison with virtual monoenergetic image (VMI) material decomposition results, we adjust the image levels to match.
Polynomial Correction (PC): A prevalent calibration technique, polynomial correction [3,19] determines combination coefficients for two calibration materials during calibration. These coefficients facilitate material decomposition.
Deep Learning Correction (DLC): Deep learning correction parallels polynomial methods by identifying coefficients for two calibration materials in the calibration phase [2], aiding material decomposition.

3.2 Calibration Results

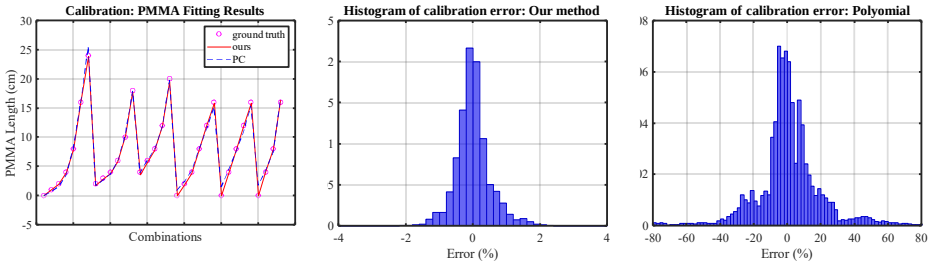

Fig. 2. Calibration results of several methods.

We conducted a series of calibration tests. These tests employed slab phantoms made from polymethyl methacrylate (PMMA) and aluminum (Al) in 33 combinations.

We derive the calibration counts, denoted as $\tilde{\Lambda}$, and conduct a comparison with the actual experimental counts and other methods. As depicted in Fig. 2, this comparison reveals that the overall error margin of our model is under 3 percent. This error level is notably low, especially when contrasted with traditional calibration methods used in PCCT systems.

3.3 Material Decomposition Results

We employed a comprehensive testing approach using a GAMMEX phantom [16], a water phantom, and a brain phantom. All tests were conducted with a rotation time of 2 seconds with a tube current of 200 mA. This variety of phantoms, each with its unique characteristics and challenges, provides a thorough testing ground to demonstrate the versatility and efficacy of our model in a range of realistic imaging scenarios.

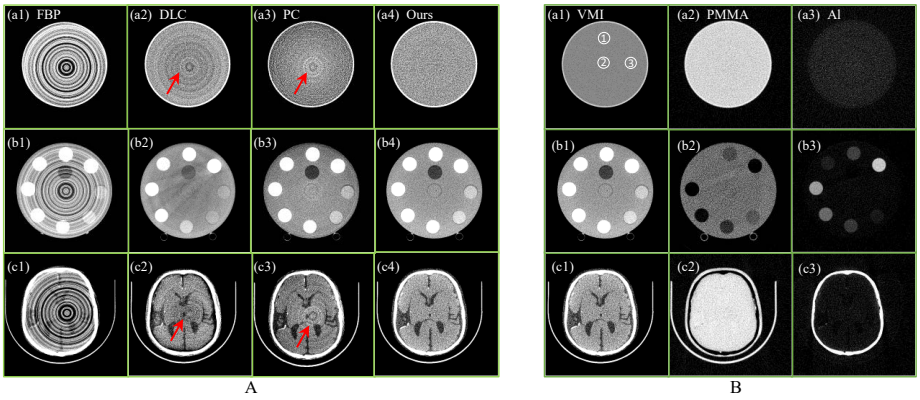

Fig. 3. Left A: 70 keV VMI results of various methods using the same data. (a) Water phantom with CT window [-40, 40] HU; (b) GAMMEX phantom with CT window [-100, 100] HU; (c) brain phantom with CT window [0, 80] HU. Right B: Material decomposition results (PMMA and Al images) of our proposed method. (a) water phantom; (b) GAMMEX phantom; (c) brain phantom.

Fig. 3A showcases the 70 keV virtual monoenergetic image (VMI) results of material decomposition for water, GAMMEX, and brain phantom, examined within a narrow CT window. A striking observation is the absence of ring artifacts in the images obtained through our proposed method, in stark contrast to the traditional filtered back-projection technique and other polynomial-based and deep-learning-based methods, which exhibit pronounced ring artifacts.

Fig. 3B displays the material decomposition outcomes for the water, brain, and GAMMEX phantom using our model. Remarkably, our model adeptly separates these phantoms into distinct images of 'soft' PMMA and 'hard' aluminum (Al), aligning closely with our physical expectations. This successful decomposition not only validates the effectiveness of our model but also illustrates its capability to accurately differentiate between materials of varying densities and compositions. Importantly, these results reveal the model's considerable potential for clinical application, suggesting its capability to accurately differentiate and visualize various tissues in medical imaging scenarios.

Table 1. Consistency check of various methods in water phantom.

	ROI 1			ROI 2			ROI 3		
	DLC	PC	Ours	DLC	PC	Ours	DLC	PC	Ours
mean (HU)	2.95	-3.56	0.62	0.80	-0.11	0.03	3.53	-3.51	0.14
std (HU)	21.11	26.30	20.67	22.30	25.94	22.02	20.46	25.74	20.72

To evaluate the reliability and accuracy of various imaging methods, we conducted a consistency check using water phantom, and regions of interest (ROIs)

are labeled in Fig. 3B water phantom. Table 1 indicates that our method exhibits a relatively lower standard deviation (std), signifying enhanced consistency. Specifically, our proposed method demonstrates a minimal bias within 1 Hounsfield Unit (HU), aligning with clinical standards. This level of precision and reliability underscores the potential of our method for clinical applications.

4 Conclusion

In summary, our method demonstrates significant promise for clinical photon counting CT applications, characterized by the absence of ring artifacts, and high accuracy in material decomposition using limited calibration samples.

Acknowledgments. The study is funded and supported by Shanghai United Imaging Healthcare Co., Ltd and Science and Technology Commission of Shanghai Municipality through "Explorer Project" (No. 22TS1400400).

Disclosure of Interests. Jinglu Ma, Guotao Quan, and Yanfeng Du in the author list are from Shanghai United Imaging Healthcare Co., Ltd. And this project is supported by Shanghai United Imaging Healthcare Co., Ltd.

References

1. Deng, K., Liu, C., Ma, R., Sun, C., Wang, X.m., Sun, X.l., et al.: Clinical evaluation of dual-energy bone removal in ct angiography of the head and neck: comparison with conventional bone-subtraction ct angiography. Clinical radiology **64**(5), 534–541 (2009)
2. Eguizabal, A., Öktem, O., Persson, M.U.: Deep learning for material decomposition in photon-counting ct. arXiv preprint arXiv:2208.03360 (2022)
3. Feng, M., Ji, X., Zhang, R., Treb, K., Dingle, A.M., Li, K.: An experimental method to correct low-frequency concentric artifacts in photon counting ct. Physics in Medicine & Biology **66**(17), 175011 (2021)
4. Jan, S., Benoit, D., Becheva, E., Carlier, T., Cassol, F., Descourt, P., Frisson, T., Grevillot, L., Guigues, L., Maigne, L., et al.: Gate v6: a major enhancement of the gate simulation platform enabling modelling of ct and radiotherapy. Physics in Medicine & Biology **56**(4), 881 (2011)
5. Johnson, T., Fink, C., Schönberg, S.O., Reiser, M.F.: Dual energy CT in clinical practice, vol. 201. Springer (2011)
6. Lee, O., Rajendran, K., Polster, C., Stierstorfer, K., Kappler, S., Leng, S., McCollough, C.H., Taguchi, K.: X-ray transmittance modeling-based material decomposition using a photon-counting detector ct system. IEEE Transactions on Radiation and Plasma Medical Sciences **5**(4), 508–516 (2020)
7. Leng, S., Bruesewitz, M., Tao, S., Rajendran, K., Halaweish, A.F., Campeau, N.G., Fletcher, J.G., McCollough, C.H.: Photon-counting detector ct: system design and clinical applications of an emerging technology. Radiographics **39**(3), 729–743 (2019)

8. Long, Y., Fessler, J.A.: Multi-material decomposition using statistical image reconstruction for spectral ct. IEEE transactions on medical imaging **33**(8), 1614–1626 (2014)
9. Mendonça, P.R., Lamb, P., Sahani, D.V.: A flexible method for multi-material decomposition of dual-energy ct images. IEEE transactions on medical imaging **33**(1), 99–116 (2013)
10. Nicolaou, S., Liang, T., Murphy, D.T., Korzan, J.R., Ouellette, H., Munk, P.: Dual-energy ct: a promising new technique for assessment of the musculoskeletal system. American Journal of Roentgenology **199**(5_supplement), S78–S86 (2012)
11. Petritsch, B., Petri, N., Weng, A.M., Petersilka, M., Allmendinger, T., Bley, T.A., Gassenmaier, T.: Photon-counting computed tomography for coronary stent imaging: in vitro evaluation of 28 coronary stents. Investigative Radiology **56**(10), 653–660 (2021)
12. Primak, A.N., Fletcher, J.G., Vrtiska, T.J., Dzyubak, O.P., Lieske, J.C., Jackson, M.E., Williams Jr, J.C., McCollough, C.H.: Noninvasive differentiation of uric acid versus non–uric acid kidney stones using dual-energy ct. Academic radiology **14**(12), 1441–1447 (2007)
13. Shen, L., Xing, Y., Zhang, L.: Joint reconstruction and spectrum refinement for photon-counting-detector spectral ct. IEEE Transactions on Medical Imaging (2023)
14. Symons, R., De Bruecker, Y., Roosen, J., Van Camp, L., Cork, T.E., Kappler, S., Ulzheimer, S., Sandfort, V., Bluemke, D.A., Pourmorteza, A.: Quarter-millimeter spectral coronary stent imaging with photon-counting ct: initial experience. Journal of cardiovascular computed tomography **12**(6), 509–515 (2018)
15. Symons, R., Krauss, B., Sahbaee, P., Cork, T.E., Lakshmanan, M.N., Bluemke, D.A., Pourmorteza, A.: Photon-counting ct for simultaneous imaging of multiple contrast agents in the abdomen: an in vivo study. Medical physics **44**(10), 5120–5127 (2017)
16. Szczykutowicz, T.P., Michaelson, B.: Using the gammex mercury 4.0™ phantom for common clinical tasks in ct. White-Paper Mercury **4** (2018)
17. Taguchi, K., Zhang, M., Frey, E.C., Xu, J., Segars, W.P., Tsui, B.M.: Image-domain material decomposition using photon-counting ct. In: Medical Imaging 2007: Physics of Medical Imaging. vol. 6510, pp. 96–107. SPIE (2007)
18. Willemink, M.J., Persson, M., Pourmorteza, A., Pelc, N.J., Fleischmann, D.: Photon-counting ct: technical principles and clinical prospects. Radiology **289**(2), 293–312 (2018)
19. Wu, D., Zhang, L., Zhu, X., Xu, X., Wang, S.: A weighted polynomial based material decomposition method for spectral x-ray ct imaging. Physics in Medicine & Biology **61**(10), 3749 (2016)
20. Zhang, Y., Mou, X., Wang, G., Yu, H.: Tensor-based dictionary learning for spectral ct reconstruction. IEEE transactions on medical imaging **36**(1), 142–154 (2016)